LBL-10207

CONF-8004 53--2

Lawrence Berkeley Laboratory

UNIVERSITY OF CALIFORNIA

Physics, Computer Science & Mathematics Division

To be presented at the 1980 International Optical Computing Conference, Washington, DC, April 7-11, 1980

LIMITED-ANGLE 3-D RECONSTRUCTIONS USING FOURIER TRANSFORM ITERATIONS AND RADON TRANSFORM ITERATIONS

Kwok-Cheong Tam and Victor Perez-Mendez

MASTER

December 1979

Prepared for the U.S. Department of Energy under Contract W-7405-ENG-48

DISTRIBUTION OF THIS DOCUMENT IS UNLIMITED

DISCLAIMER

[illegible]

231-16

LBL10207

Limited-angle 3-D reconstructions using Fourier transform iterations and Radon transform iterations

Kwok-Cheong Tam and Victor Perez-Mendez

Lawrence Berkeley Laboratory, Berkeley, California 94720 and
Department of Radiology, University of California, San Francisco,
San Francisco, California 94143

Abstract

The principles of limited-angle reconstruction of space-limited objects using the concepts of "allowed cone" and "missing cone" in Fourier space are discussed. The distortion of a point source resulting from setting the Fourier components in the missing cone to zero has been calculated mathematically, and its bearing on the convergence of an iteration scheme involving Fourier transforms has been analysed in detail. It was found that the convergence rate is fairly insensitive to the position of the point source within the boundary of the object, apart from an edge effect which tends to enhance some parts of the boundary in reconstructing the object. Another iteration scheme involving Radon transforms was introduced and compared to the Fourier transform method in such areas as root mean square error, stability with respect to noise, and computer reconstruction time.

Introduction

Many imaging devices, such as planar positron cameras, electron microscopes, radiotelescopes, etc., view an object only from a limited angular range. As shown in our previous papers,[1,2] the only Fourier components of the object that can be determined directly under these circumstances are those inside the "allowed cone," which is the region in Fourier space where the optical transfer function of the system is non-zero. Figure 1 shows the shape of the space-invariant point response function and optical transfer function for a typical limited-angle imaging system. Fourier space is partitioned into an "allowed cone" and a "missing cone" according to whether the optical transfer function is zero or not.

In Reference 1, an iteration scheme was introduced to recover the Fourier components of the object in the missing cone. The scheme, which is illustrated in Figure 2, makes use of the knowledge of the finite extent of the object to fill in the missing-cone components. Some properties of the iteration scheme, such as convergence and error propagation, have been analysed in Reference 2. In this paper the spatial uniformity of the reconstructed object is studied by considering the effect of the missing cone on point sources. Another iteration scheme for limited-angle reconstruction involving Radon transforms is described and compared with the present one involving Fourier transforms. Throughout the paper the axis of the allowed cone is assumed to lie along the k_x-axis, and the cone has a half-angle θ_0 (see Figure 2).

Spatial Uniformity

The effect of setting the missing-cone components to zero on a point source has been mentioned in previous papers.[2,3] In this section this effect is analysed in more detail in two dimensions. Besides casting light on the nature of the distortion caused by the missing cone, results of the analysis are also useful in understanding the spatial uniformity of reconstructed objects.

Assume a point source is located at the origin $x = z = 0$. With the Fourier components in the missing cone set to zero, the distorted point source $\rho'(x,z)$ is given by

$$\rho'(x,z) = \int_{-\infty}^{\infty} dk_x \exp(-2\pi i k_x x) \int_{-|k_x|\tan\theta_0}^{|k_x|\tan\theta_0} dk_z \exp(-2\pi i k_z z) \tag{1}$$

Treating the integrands as generalized functions,[4] we get, by integrating,

$$\rho'(x,z) = \frac{1}{\pi^2(\tan\theta_0 z^2 - \frac{x^2}{\tan\theta_0})} \quad \text{for } (x,y) \neq (0,0) \tag{2}$$

The distortion as expressed by Equation (2) possess the antisymmetry property with respect to the interchanges: $x \leftrightarrow z$, $\tan\theta_0 \leftrightarrow 1/\tan\theta_0$. This is to be expected from the complementary nature of the allowed and missing cones.

Equation (2) also shows that the distortion is positive in the cones $|x| < \tan\theta_0|z|$, and negative in the cones $|x| > \tan\theta_0|z|$. In an extended object, most of the negative distortion will be swamped by the positive densities at other positions in the object. Therefore, the use of a positivity constraint in iterations, i.e. resetting all negative densities to zero, improves convergence significantly for point sources but not for extended objects, as reported in a previous paper.[2] The positivity constraint was utilized in all subsequent iterations in this paper.

The positive distortion in the region $|x| < \tan\theta_0|z|$ rises to high positive values in the immediate vicinity of the lines $x = \pm \tan\theta_0 z$; the negative distortion in the region $|x| > \tan\theta_0|z|$ also becomes large near the lines. These high positive and negative values give rise to what appear to be four ridges originating from the point source and decaying with distance: two positive ones and two negative ones bordering the lines $x = \pm \tan\theta_0 z$. These distortions are singular and discontinuous in crossing the boundary between the positive and negative regions. These singularities and discontinuities are smeared out in digital Fourier transformation and averaged out to small finite values.

The positive distortion in the cones $|x| < \tan\theta_0|z|$ makes the point source appear elongated in the z direction. Elongation along the z-axis ($x = 0$) is especially serious when the half-angle θ_0 of the allowed cone is small, as implied in Equation (2).

The distortion of a point source caused by the missing-cone components is illustrated pictorially in Figure 3. The half-angle of the allowed cone is $\tan^{-1}(0.5)$. Figure 3A shows the positive density distribution of the distorted point source, and Figure 3B shows the negative density distribution. The presence of the two positive and the two negative ridges originating from the point source, and the elongation of the point source along the z-axis are evident. The other smaller ridges not originating from the point source are due to the sharp cut-off of the Fourier area.

At small angle θ_0, most of the distortion energy of the distorted point source resides in the elongated portion along the z-axis, where the amplitude is highest. If part or all of this elongation is repeatedly reset to zero during iterations, convergence will be very rapid. Thus, at small allowed-cone angles, convergence of the iteration scheme is primarily determined by whether or not the point source is located in a position where part or all of its elongation extends outside the object boundary and thus is repeatedly reset to zero during iterations.

The above discussion can be made clear by considering the situation in Figure 4. The 32 x 32 array is the reconstruction area, while the 11 x 11 square area in the middle of the array represents the finite extent of an object: anything outside the square is reset to zero during iterations. As far as the convergence of the iterations is concerned, the pixel A(16,17) in Figure 4 is the worst location within the square boundary because a point source at this position has the largest fraction of its ridges inside the square boundary, whereas pixel B(16,22), similar to the other pixels on the top and bottom edges, represents the best location, since half of each ridge is outside the boundary for a point source located at B. For pixel C(21,17) and the other pixels on the left and right edges, half of each ridge is also outside the boundary, but all of the elongated portion is still inside; thus a point source at C is not expected to do much better than at A.

To verify these points, a point source with an allowed cone of half-angle $\tan^{-1}(0.5)$ was reconstructed through iterations at the locations A, B, and C, respectively. The results are presented in Figures 5-7. Part A of each figure shows the individual point source with missing-cone components set to zero, and the improved point source after 20 iterations is shown in part B. In these figures all the negative densities have been set to zero, and the densities have been scaled to give the minimum root mean square error σ from the original point source taken over the square boundary. While the quality of the reconstructed point source at B is much better than that at A, the one at C is only slightly better. These results show that at small angles the elongated portion along the z-axis is the main factor determining the convergence of the iterations, and thus the pixels on the top and bottom edges of the square boundary will reconstruct much better than the others.

Fortunately this edge effect is very localized at the top and bottom boundaries. To show this, a missing-cone point source was reconstructed at position D, in the vicinity of B and further into the interior of the boundary. The result was very similar to that of A and C. The values of the root mean square error, σ, of the missing-cone point sources before and after iterations taken over the area enclosed by the square boundary for the positions A, B, C, and D are tabulated in Table 1.

As the angle of the allowed cone increases, the distortion amplitude becomes more spread out in the ridges and the x-axis. As a result, more pixels near the boundary will be reconstructed better than the interior pixels. However, since the convergence of the iteration scheme improves rapidly with the increase in the allowed-cone angle,[2] the reconstruction

T/M1

error would be small everywhere within the object boundary, and thus could not cause any serious problem in spatial uniformity.

Table 1. Values of σ taken over the area enclosed by the square boundary for various positions of the point source

Position	σ (arbitrary units) before iterations	after 20 iterations
A	0.803	0.659
B	0.699	0.334
C	0.793	0.610
D	0.783	0.643

Radon transform iteration scheme

The iteration scheme described above Fourier transforms the object back and forth between the object space and the Fourier space, the constraints used being the known Fourier components inside the allowed cone, and the known finite extent of the object. An alternate approach to object reconstruction from limited-angle information is to apply Radon transforms and manipulate the object back and forth between the object space and projection space, the constraints used in this case being the projections in the limited angular range and the known finite extent of the object. We have been trying to improve the performance of the iteration scheme for limited-angle reconstruction; the alternative method involving Ra n transforms represents such an attempt, which is motivated in part by the success of other workers in performing complete-angle image reconstructions in object space.

The Radon transform iteration scheme is shown in Figure 8. Inverse Radon transformation is achieved through convolution with the kernel developed by Shepp and Logan.[5] Since there is a one-to-one correspondence between projections of a function and lines of Fourier components of the function passing through the origin in the Fourier space,[6] the convergence of the Fourier transform iteration scheme ensures that of the Radon transform iteration scheme.

The Radon transform iteration scheme was applied to reconstruct a point source located at position A in Figure 4. The total number of projections uniformly generated between zero and π is 17. This number was chosen according to the sampling criteria of Klug and Crowther,[7] and so the projections contain all the information necessary to reconstruct the object up to the bandwidth imposed by the grid size. Out of the 17, only five projections which lie within a cone of half-angle $\tan^{-1}(0.5)$ oriented along the z-axis were used in reconstructing the point source.

The results are summarized in Table 2, which shows the root mean square error σ of the reconstructed point source after 20 iterations taken over the area enclosed by the square boundary for various additive noise levels in the projections. Also shown in Table 2 for comparison purposes are the corresponding results of reconstructing from the same five projections through the Fourier transform iteration scheme, the Fourier components inside the allowed cone being obtained through deconvolution.[4] As far as the quality of the reconstructions and stability with respect to noise are concerned, Table 2 shows that the Radon scheme is a feasible alternative. That this scheme gave slightly inferior results to that of the Fourier scheme is due to the fact that digital Fourier transform and inverse transform are exact inverses of each other, whereas the digital Radon transform and inverse transform are not. As for computer time, the availability of fast Fourier transform subroutines gives the Fourier scheme advantage over the Radon scheme, especially when there are large numbers of projections involved. For the subroutines that were used in our works involving a 32 x 32 array, one cycle of Fourier transform iteration used 11 msec on a CDC 7600 machine, whereas the computer time for one cycle of the Radon transform iteration involving 17 projections was about 350 msec.

Table 2. Comparison between the Radon transform iterations and the Fourier transform iterations.

Noise level (%)	σ after 20 iterations (arbitrary units) Radon transform iterations	Fourier transform iterations
0	0.757	0.668
± 10	0.775	0.688
± 40	0.865	0.828

Discussion

We have demonstrated that the Fourier transform iteration scheme gives spatially-uniform reconstruction across an object. The Radon transform iteration scheme was shown to

be practical, but because of the much longer computer time required, the Fourier transform method is preferable.

Acknowledgments

This work was supported by the Physics Division of the U. S. Department of Energy under contract No. W-7405-ENG-48.

References

1. Tam, K. C., Perez-Mendez, V., and Macdonald, B., IEEE Trans. Nucl. Sci., NS-26 (1979) 2797.
2. Tam, K. C., Perez-Mendez, V., and Macdonald, B., IEEE Trans. Nucl. Sci., NS-27 (1980).
3. Chiu, M. Y., Barrett, H. H., Simpson, R. G., Chou, C., Arendt, J. W., and Gindi, G. R., J. Opt. Soc. Am., 69 (1979) 1323.
4. Papoulis, A., The Fourier Integral and Its Applications (New York: McGraw-Hill), 1962, p. 269
5. Shepp, L. A., and Logan, B. F., IEEE Trans. Nucl. Sci., NS-21 (1974) 21.
6. Crowther, R. A., DeRosier, D. J., and Klug, A., Proc. R. Soc. Lond. A, 317 (1970) 319.
7. Klug, A., and Crowther, R. A., Nature, 238 (1972) 435.
8. Tam, K. C., Chu, G., Perez-Mendez, V., and Lim, B. C., IEEE Trans. Nucl. Sci., NS-25 (1978) 152.

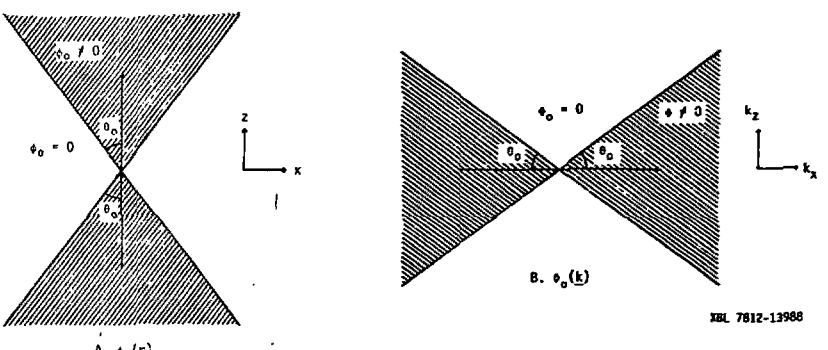

Figure 1. A 2-D point response function $\phi_o(\underline{r})$ and its optical transfer function $\Phi_o(\underline{k})$.

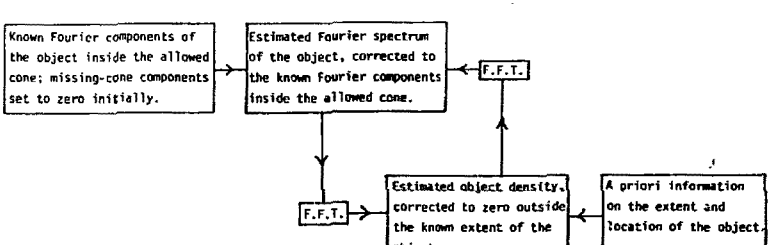

Figure 2. Fourier transform iteration scheme for filling in missing-cone Fourier components.

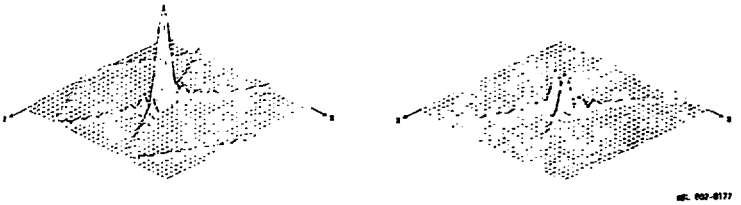

A. POSITIVE DENSITY DISTRIBUTION

B. NEGATIVE DENSITY DISTRIBUTION

Figure 3. Positive and negative density distributions of a point source whose missing-cone Fourier components have been set to zero.

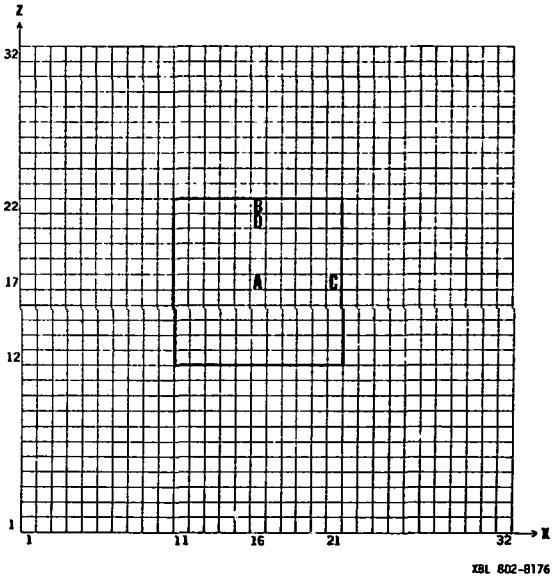

Figure 4. A 11 x 11 square boundary representing the finite extent of an object within a 32 x 32 reconstruction area.

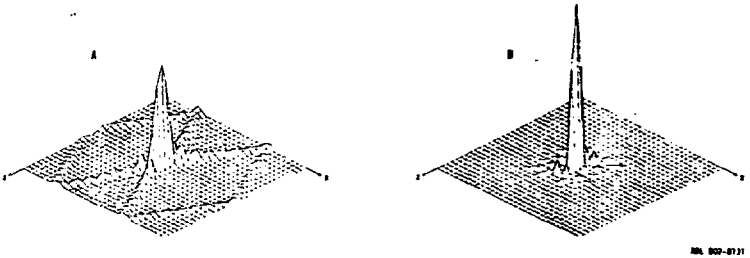

Figure 5. A missing-cone point source at the center of the square boundary. The half-angle of the allowed cone is $\tan^{-1}(0.5)$.
A. No iterations. B. After 20 iterations.

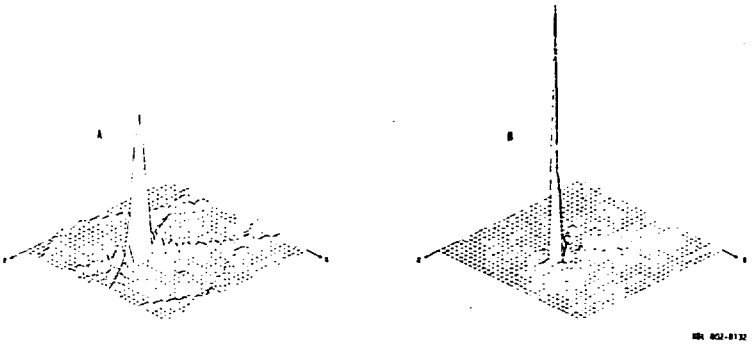

Figure 6. A missing-cone point source on the top edge of the square boundary. The half-angle of the allowed cone is $\tan^{-1}(0.5)$.
A. No iterations. B. After 20 iterations.

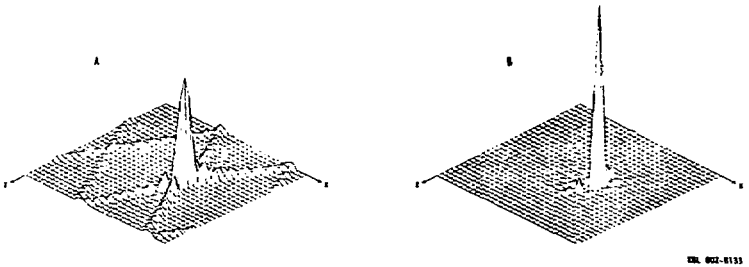

Figure 7. A missing-cone point source on a side edge of the square boundary. The half-angle of the allowed cone is $\tan^{-1}(0.5)$.
A. No iterations. B. After 20 iterations.

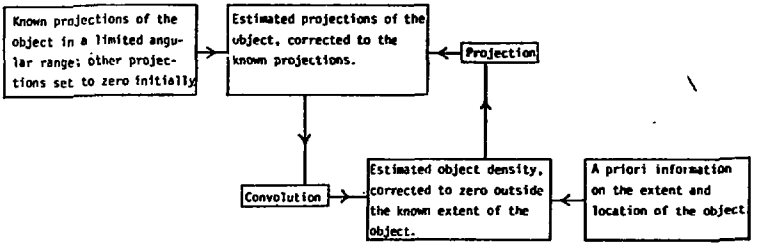

Figure 8. Radon transform iteration scheme for filling missing projections.

TAM 7